Supporting Information

Interfacing boron monophosphide with molybdenum disulphide for an ultrahigh performance in thermoelectrics, 2D excitonic solar cells and nanopiezotronics

Manish Kumar Mohanta, Ashima Rawat, Nityasagar Jena, Dimple, Raihan Ahammed and Abir De Sarkar*

Institute of Nano Science and Technology, Phase 10, Sector 64, Mohali, Punjab-160062, India

*E-mail: abir@inst.ac.in; abirdesarkar@gmail.com

The piezoelectric stress coefficient/tensor, e_{ij}, which relates the polarization P_i to the applied strain ε_j is given by $P_i = \sum_j e_{ij}\varepsilon_j$ can be directly obtained from first-principle calculations. Instead of the piezoelectric stress tensor (e_{ij}), piezoelectric strain tensor d_{ij} is of greater importance in ultrathin 2D materials. It relates the induced polarization to the applied stress, $P_i = \sum_j d_{ij}\sigma_j$ (I) and is more straight forward in ultra-thin circuit designs.[1] Linear piezoelectric coefficients e_{ijk} and d_{ijk} are the third rank tensors that couple electronic polarization (P_i) or the macroscopic electric field (E_i) to the second-rank stress tensor (σ_{jk}) or the strain tensor (ε_{jk}) as given by:

$$d_{ijk} = \left(\frac{\partial P_i}{\partial \sigma_{jk}}\right)_{E,T} = \left(\frac{\partial \varepsilon_{ij}}{\partial E_k}\right)_{\sigma,T} \quad \text{(II)}$$

$$e_{ijk} = \left(\frac{\partial P_i}{\partial \varepsilon_{jk}}\right)_{E,T} = -\left(\frac{\partial \sigma_{jk}}{\partial E_i}\right)_{\varepsilon,T} \quad \text{(III)}$$

where $i, j, k \in \{1, 2, 3\}$ corresponds to x, y, z direction respectively.

Further piezoelectric coefficients are defined as

$$e_{ijk} = \frac{\partial P_i}{\partial \varepsilon_{jk}} = e_{ijk}^{elc} + e_{ijk}^{ion} \quad \text{(IV)}$$

$$d_{ijk} = \frac{\partial P_i}{\partial \sigma_{jk}} = d_{ijk}^{elc} + d_{ijk}^{ion} \quad \text{(V)}$$

In contrast, the relaxed-ion piezoelectric tensors $e_{ijk}(d_{ijk})$ are obtained from the sum of ionic and electronic contributions with the fully relaxed ionic positions. The relaxed-ion coefficients would be more reliable because they are experimentally relevant. The symmetry of the material reduces when we thinned down to monolayers. Hence, the stress/strain tensor of rank three reduces to rank two. Combining the relation between piezoelectric stress and strain coefficients, e_{ik} and d_{ij} and elastic stiffness coefficients C_{jk} for 2D material: $e_{ik} = d_{ij}C_{jk}$ where i = 1, 2, 3 represents x, y, z-direction and for j, k we have used Voigt notation[2]; 1 = xx, 2 = yy, 3 = zz, 4 = yz, 5 = zx, 6 = xy.

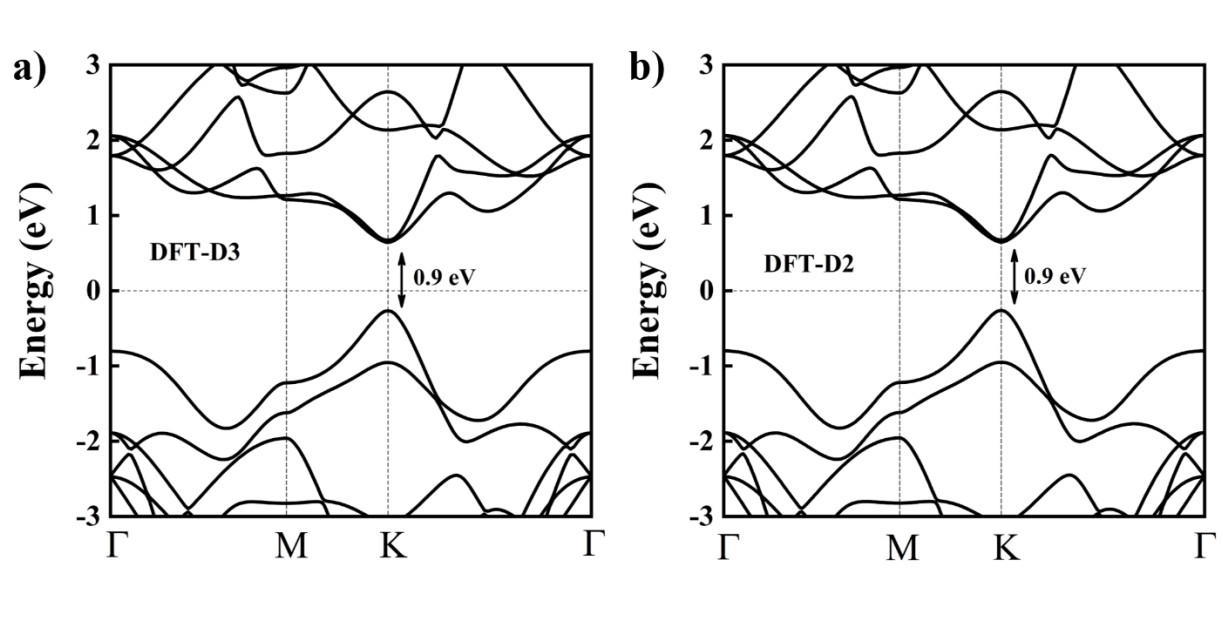

Figure S1: Calculated electronic dispersion of MoS_2/BP using GGA-PBE with (a) DFT-D3 and (b) DFT-D2.

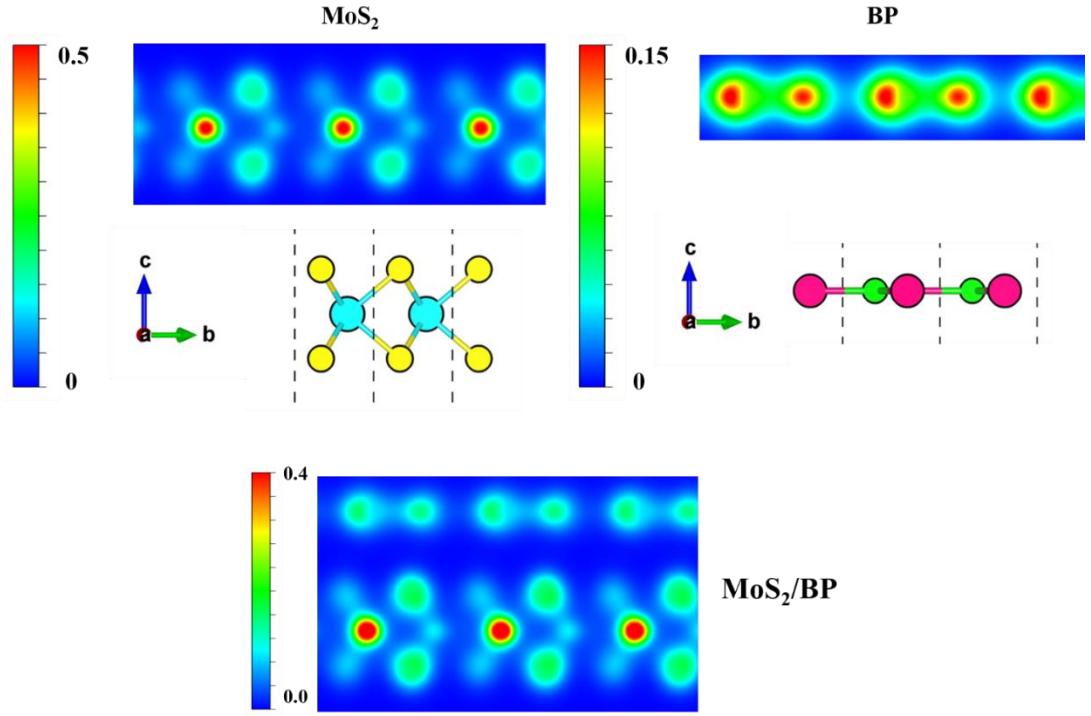

Figure S2: Charge density contour maps (e/Å^3) for pristine monolayer MoS_2, BP and their heterobilayer.

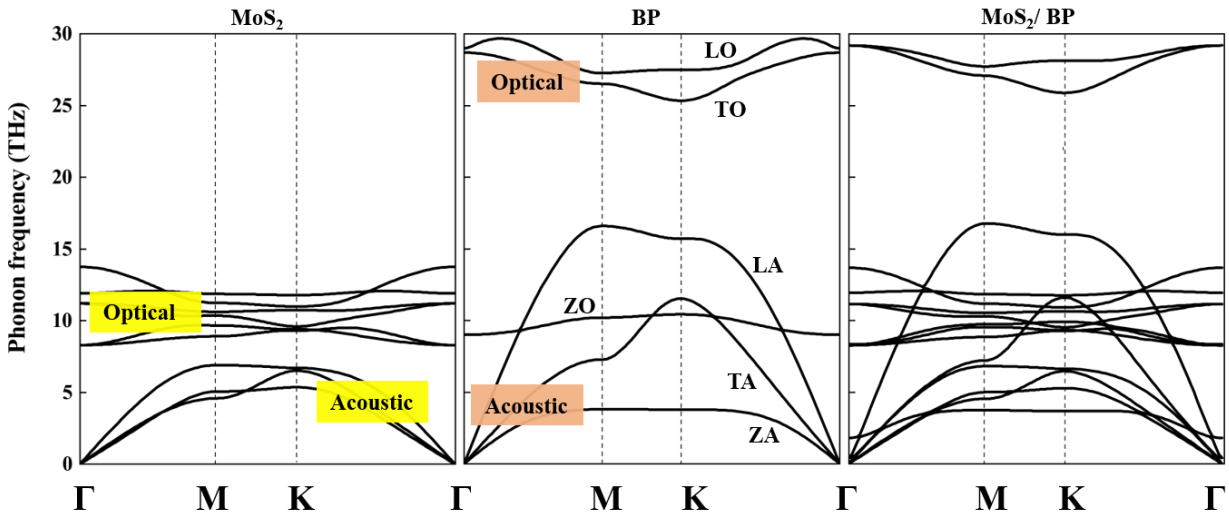

Figure S3: Phonon dispersion of individual and heterobilayer

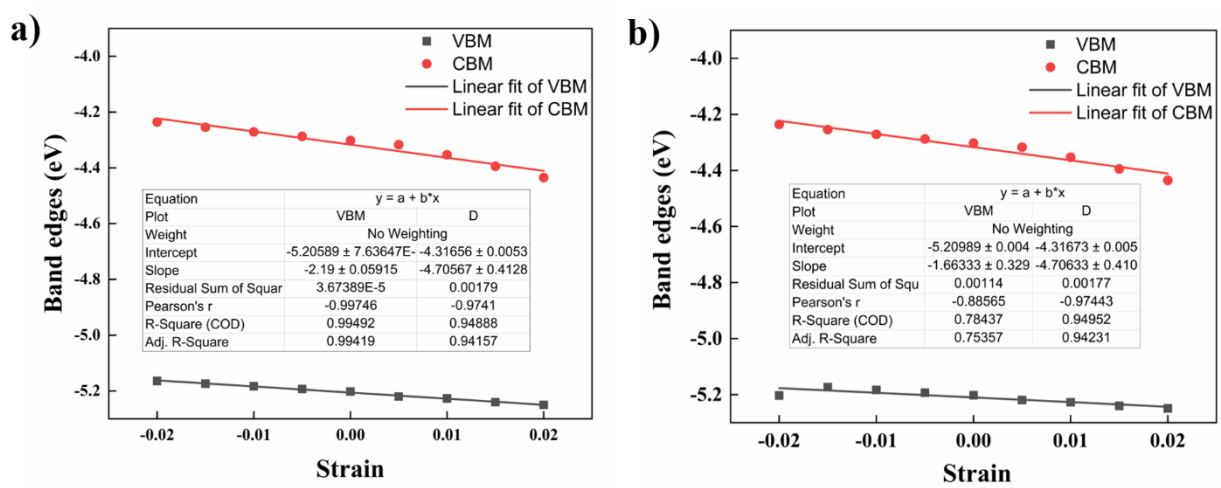

Figure S4: (a) CBM and VBM as a function of uniaxial compression or tension of MoS_2/BP along K-Γ direction, (b) K-M direction.

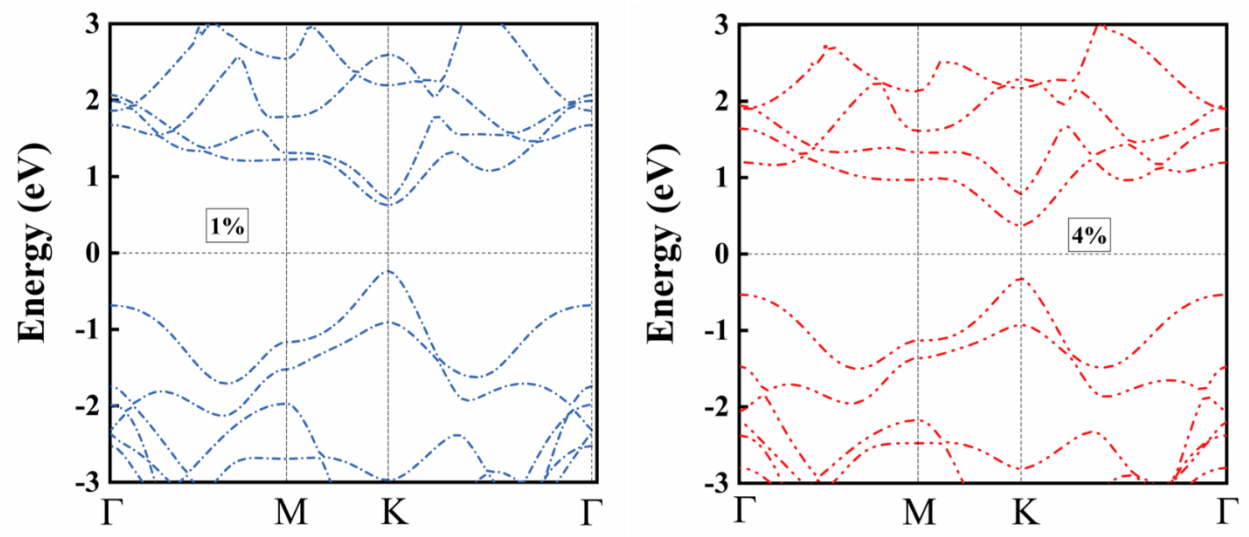

Figure S5: Evolution in the electronic band dispersion in the MoS_2/BP heterobilayer with the application of biaxial tensile strain based on GGA-PBE. The bands arising from the individual monolayers are shown in Fig. 2(c). The conduction band offset (CBO) is found to increase with the magnitude of biaxial strain.

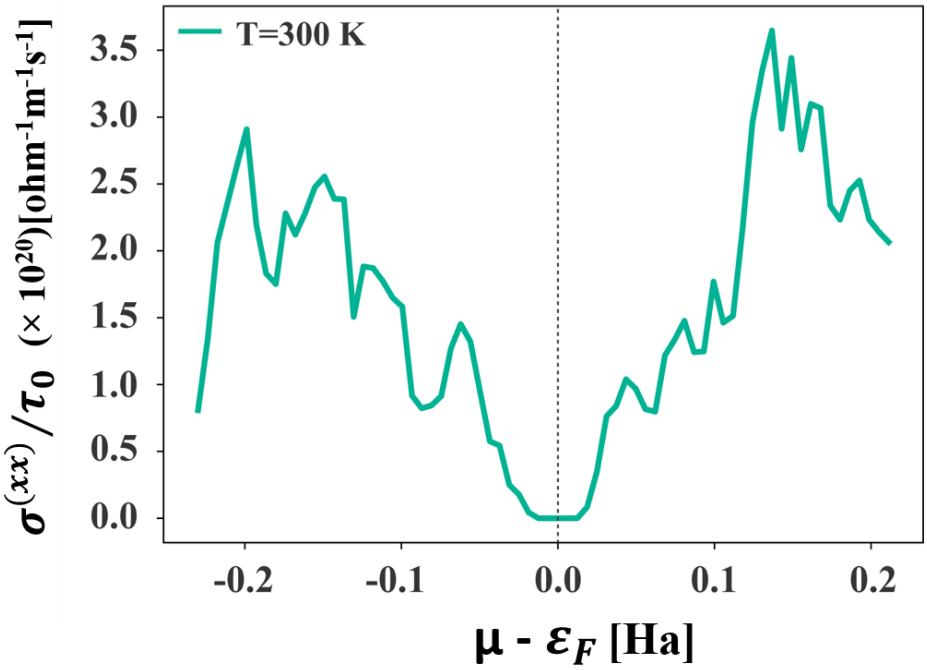

Figure S6: Calculated plot of electrical conductivity of the MoS_2/BP vdW heterobilayer as a function of chemical potential.

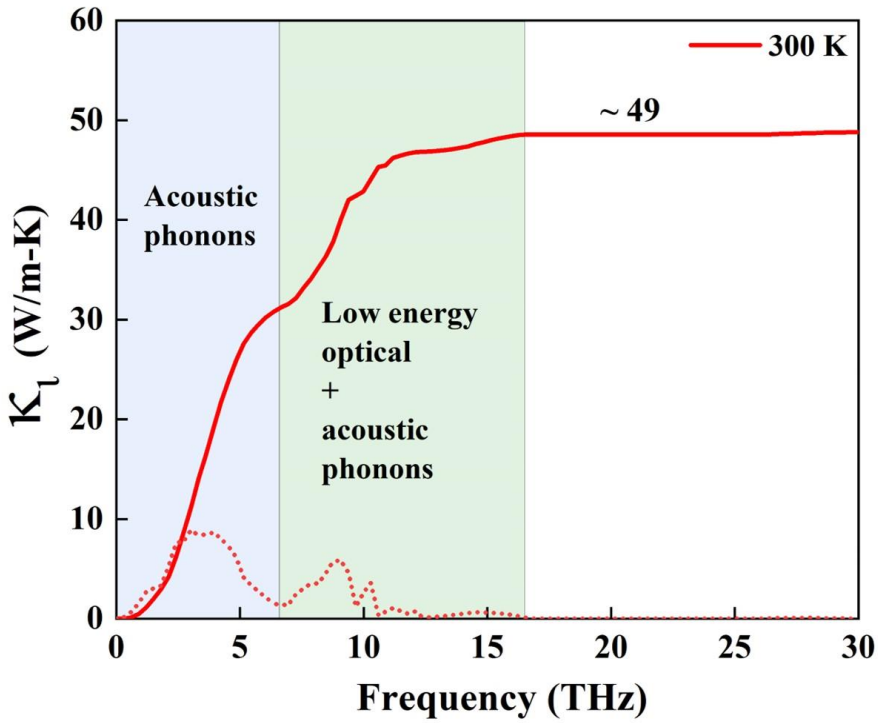

Figure S7: Cumulative lattice thermal conductivity (red solid line) and its derivative (red dash line) at 300K with contribution of low energy optical mode and acoustic mode towards the total lattice thermal conductivity.

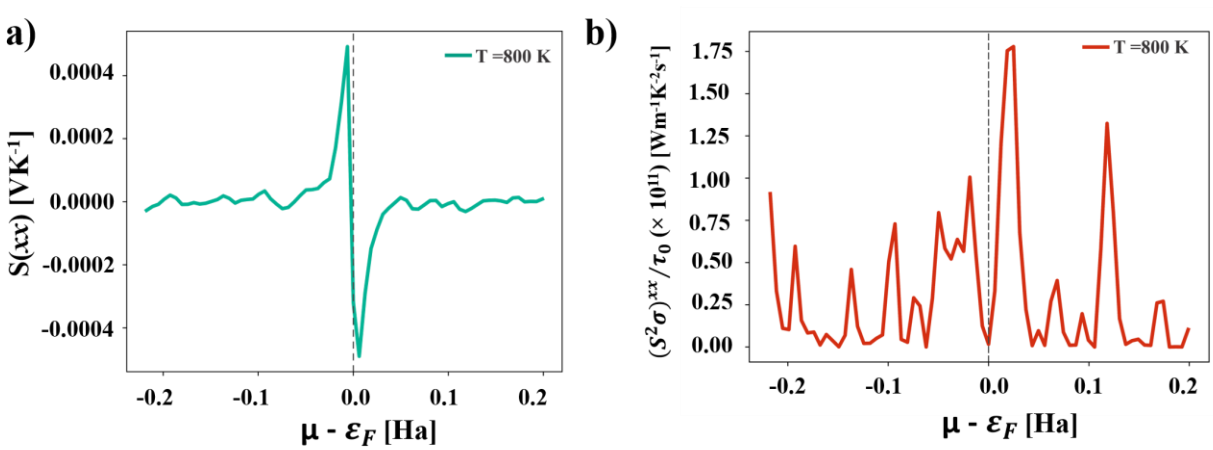

Figure S8: Calculated (a) Seebeck coefficient and (b) thermoelectric power factor at 800 K for MoS_2/BP heterobilayer as a function of chemical potential

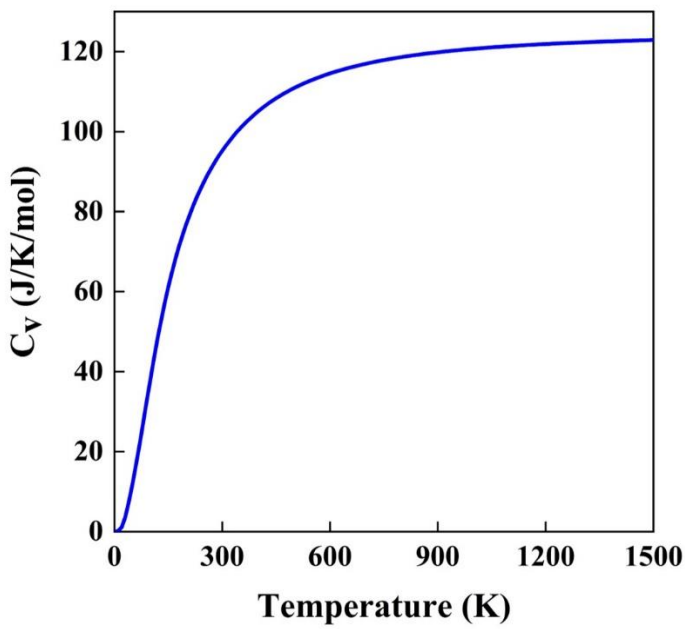

Figure S9: Calculated volumetric heat capacity as a function of temperature

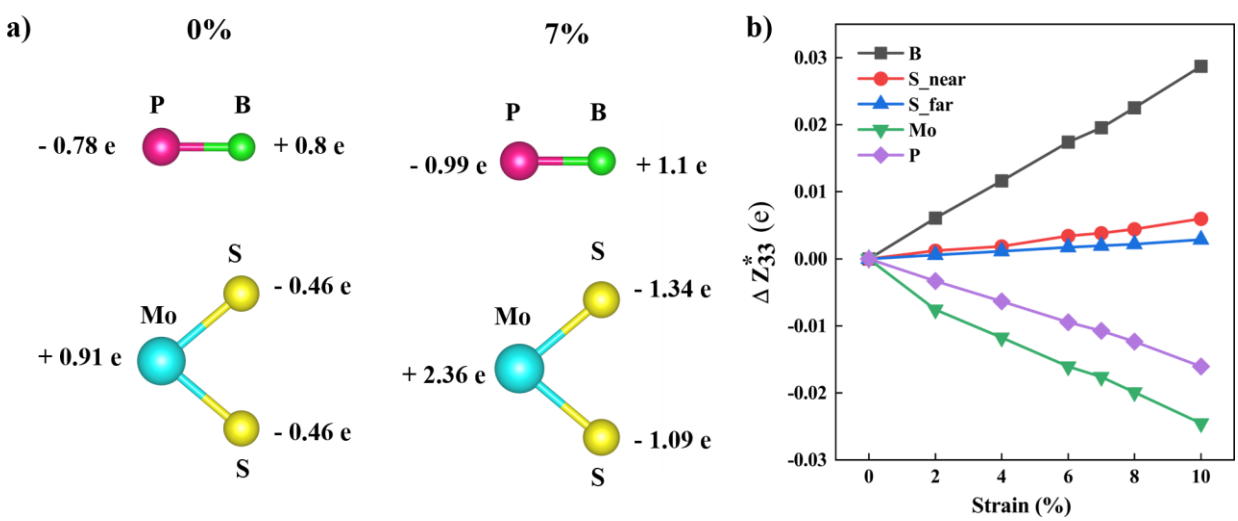

Figure S10: (a) Bader atomic charges at different % of vertical compressive strain of MoS_2/BP (stacking I), (b) Variation in the change in Born effective charges on B, Mo, P and the S ions along the z-direction (ΔZ^*_{33}) relative to the pristine, unstrained hetero-bilayer with the application of vertical compressive strain. S_near and S_far denote S ion near to and far from the BP monolayer.

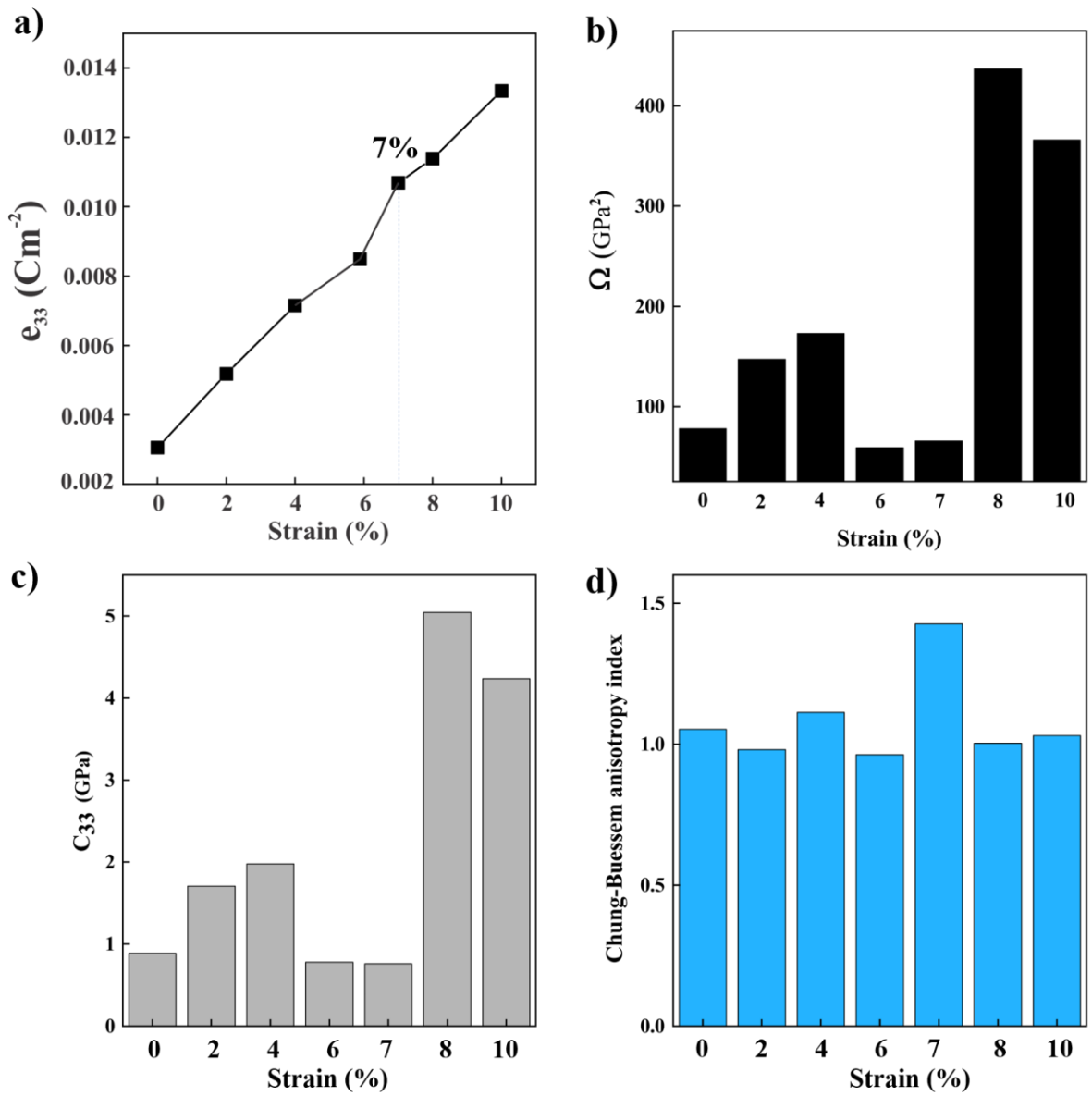

Figure S11: Variation in (a) piezoelectric stress tensor, (b) $\Omega = (C_{11} + C_{12})C_{33} - 2C_{13}^2$, (c) C_{33} and (d) Chung-Buessem anisotropy index (for anisotropy in elastic stiffness) in the heterobilayer with vertical compressive strain.

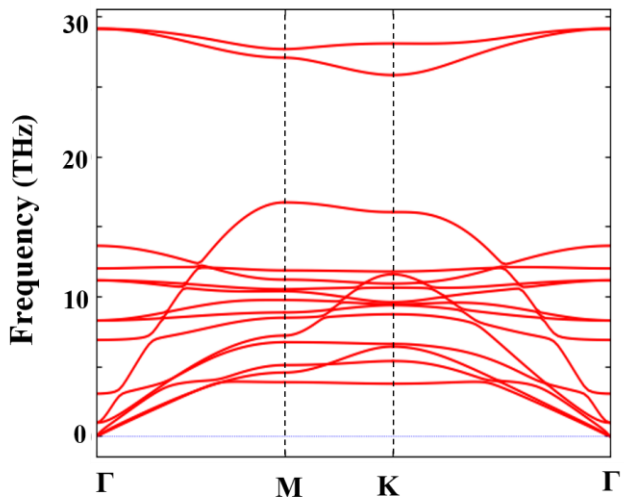

Figure S12: Phonon dispersion of 7% vertical compressive strain MoS_2/BP heterobilayer.

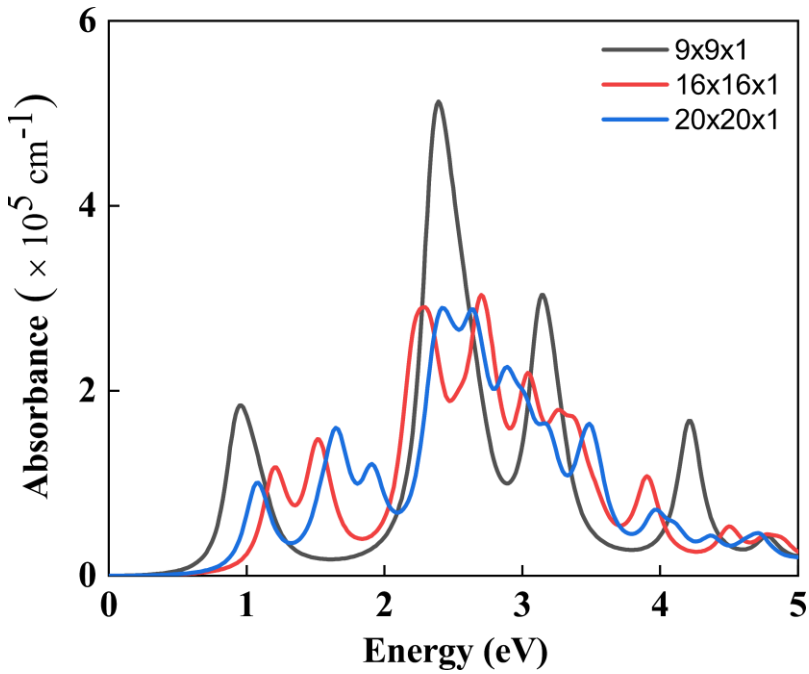

Figure S13: The calculated absorption spectra of *h*-BP monolayer with different *k*-mesh sampling. A 9x9x1 k-mesh was used in an earlier work.[3]

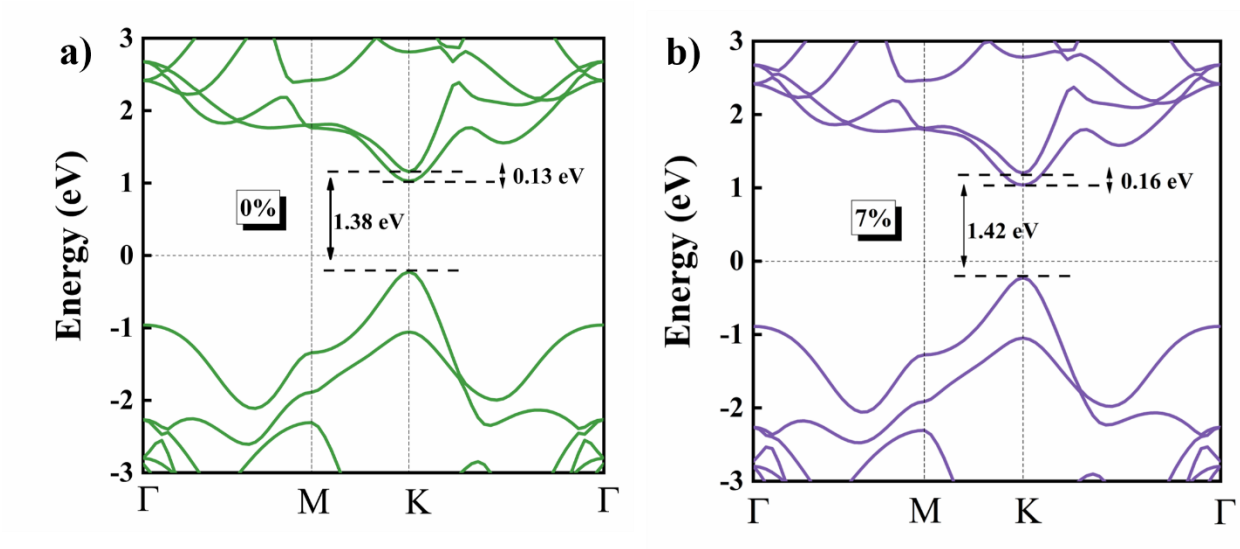

Figure S14: Electronic band dispersion (HSE06) of MoS_2/BP (a) unstrained and (b) 7 % vertical compressive strain. The bands arising from the individual monolayers are shown in Fig. 2(c). The conduction band offset (CBO) changes marginally with the application of vertical compressive strain.

Table-S1 Calculated effective mass (m^*), deformation potential constant E_i (eV) and carrier mobility μ ($cm^2V^{-1}s^{-1}$) for electrons and holes along high symmetric directions of MoS_2 and BP monolayers at 300 K

Monolayer	Direction	Carrier type	$\lvert m^*/m_o \rvert$	$\lvert E_i \rvert$	μ (*10^3)
MoS_2	$K \rightarrow \Gamma$	Electron	0.535	9.33	0.141
		Hole	0.719	4.93	0.299
	$K \rightarrow M$	Electron	0.476	9.33	0.158
		Hole	0.561	4.93	0.383
BP	$K \rightarrow \Gamma$	Electron	0.224	0.94	57.74
		Hole	0.217	2.45	9.39
	$K \rightarrow M$	Electron	0.373	0.96	34.31
		Hole	0.313	2.62	6.2

Table-S2 Calculated optimized geometrical parameters of the hetero-bilayer: equilibrium distance, binding energy (DFT-D3)		
MoS_2/BP	**d_0(Å)**	**Binding energy (meV/Å^2)**
II	3.2	-22.3
III	3.6	-17.48
IV	3.57	-18.37

Table-S3 Calculated relaxed ion (Electronic + Ionic) piezoelectric tensor e_{ij} (unit: C/m^2) and total elastic modulus C_{ij} (unit: GPa) of MoS_2/BP heterobilayer							
e_{ij}				C_{ij}			
	1	**2**	**3**		**1**	**2**	**3**
1	-	-	-	**1**	69.17	18.5	-0.06
2	0.0251	-0.0256	-0.0006	**2**	18.5	69	0.11
3	0.001	0.001	0.003	**3**	-0.06	0.11	0.88

Table-S4 Born effective charges on each ionic species in pristine/unstrained heterobilayer					
	Stacking	Atoms	Born effective charges		
			XX	**YY**	**ZZ**
Pristine		Mo	-1	-1	-0.08
		S	0.5	0.5	0.001
		B	1.58	1.59	-0.02
		P	-1.58	-1.59	0.02
Heterobilayer	I	Mo	-0.95	-0.95	-0.12
		S	0.43	0.43	0.07
		B	1.79	1.8	0.007
		P	-1.75	-1.77	-0.005
	II	Mo	-0.99	-0.99	-0.1
		S	0.45	0.45	0.067
		B	1.83	1.83	-0.02
		P	-1.76	-1.75	0.007
	III	Mo	-0.91	-0.92	-0.1
		S	0.47	0.48	0.063
		B	1.77	1.77	-0.04
		P	-1.81	-1.81	0.03
	IV	Mo	-0.9	-0.9	-0.11
		S	0.44	0.45	0.07
		B	1.7	1.71	-0.043
		P	-1.72	-1.74	0.39

Born effective charge (BEC) tensors, Z^*_{ij} provide microscopic insight into the piezoelectric coefficients via changes in intrinsic polarization (P_i) in the system. $Z^*_{ij} = \Omega_0 \frac{\partial P_i}{\partial u_j}$ (VI) , where i, j = x, y, z direction and Ω_0 is the unit cell volume, u is the displacement of the atom along a particular direction.

Table-S5 Born effective charges on each ionic species along z direction in unstrained/strained condition		
Heterobilayer	Atoms	Born effective charges along the *z* direction (Z^*_{zz} or, Z^*_{33})
BP/MoS_2 (pristine/unstrained)	B	0.0075
	P	-0.0054
	Mo	-0.12
	S	0.047
	S	0.07
BP/MoS_2 (7 % compressive strain)	B	0.027
	P	-0.016
	Mo	-0.134
	S	0.049
	S	0.074

Table-S6 Calculated elastic constants C_{11}, C_{22}, C_{12} (N/m), Young's modulus Y (N/m), shear moduli G_{xy} (N/m), Poisson's ratio (v) in 7% strained MoS_2/BP calculated using AELAS code[4]

System	C_{11}	C_{22}	C_{12}	Y_x	Y_y	G_{xy}	v_x	v_y	**Status**
MoS_2/BP	310.98	310.98	75.86	292.47	292.47	117.56	0.24	0.24	Stable

References:

(1) Zhou, Y.; Wu, D.; Zhu, Y.; Cho, Y.; He, Q.; Yang, X.; Herrera, K.; Chu, Z.; Han, Y.; Downer, M. C.; et al. Out-of-Plane Piezoelectricity and Ferroelectricity in Layered α-In2Se3 Nanoflakes. *Nano Lett.* **2017**, *17* (9), 5508–5513. https://doi.org/10.1021/acs.nanolett.7b02198.

(2) Yin, H.; Gao, J.; Zheng, G.-P.; Wang, Y.; Ma, Y. Giant Piezoelectric Effects in Monolayer Group-V Binary Compounds with Honeycomb Phases: A First-Principles Prediction. *J. Phys. Chem. C* **2017**, *121* (45), 25576–25584. https://doi.org/10.1021/acs.jpcc.7b08822.

(3) Mohanta, M. K.; Rawat, A.; Dimple; Jena, N.; Ahammed, R.; De Sarkar, A. Superhigh Out-of-Plane Piezoelectricity, Low Thermal Conductivity and Photocatalytic Abilities in Ultrathin 2D van Der Waals Heterostructures of Boron Monophosphide and Gallium Nitride. *Nanoscale* **2019**, *11* (45), 21880–21890. https://doi.org/10.1039/C9NR07586K.

(4) Zhang, S. H.; Zhang, R. F. AELAS: Automatic ELAStic Property Derivations via High-Throughput First-Principles Computation. *Computer Physics Communications* **2017**, *220*, 403–416. https://doi.org/10.1016/j.cpc.2017.07.020.